Color Demosaicking via Directional Linear Minimum Mean Square-Error Estimation

Lei Zhang and Xiaolin Wu[*], *Senior Member, IEEE*

Dept. of Electrical and Computer Engineering, McMaster University

Email: {johnray, xwu}@mail.ece.mcmaster.ca

Abstract-- Digital color cameras sample scenes using a color filter array of mosaic pattern (e.g. the Bayer pattern). The demosaicking of the color samples is critical to the quality of digital photography. This paper presents a new color demosaicking technique of optimal directional filtering of the green-red and green-blue difference signals. Under the assumption that the primary difference signals (PDS) between the green and red/blue channels are low-pass, the missing green samples are adaptively estimated in both horizontal and vertical directions by the linear minimum mean square-error estimation (LMMSE) technique. These directional estimates are then optimally fused to further improve the green estimates. Finally, guided by the demosaicked full-resolution green channel, the other two color channels are reconstructed from the LMMSE filtered and fused PDS. The experimental results show that the presented color demosaicking technique significantly outperforms the existing methods both in PSNR measure and visual perception.

Index Terms: Color demosaicking, Bayer color filter array, LMMSE, directional filtering.

EDICS: 4-COLR, 2-COLO.

I. Introduction

Most digital cameras capture an image with a single sensor array. At each pixel, only one of the three primary colors (red, green and blue) is sampled. Fig. 1 shows the commonly used Bayer color filter array (CFA) [5]. In order to reconstruct a full color image the missing color samples need to be interpolated by a process called color demosaicking. The quality of reconstructed color images depends on the image contents and the employed demosaicking algorithms [15].
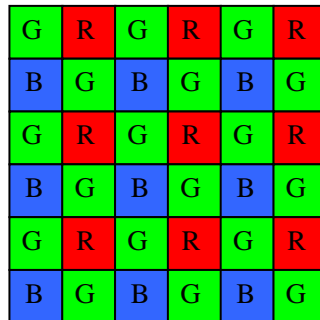

Figure 1. The Bayer pattern.

The early demosaicking methods include nearest neighbor replication, bilinear interpolation and cubic B-spline interpolation [1,10, 15]. These methods can be simply implemented but they suffer from many artifacts such as blocking, blurring and zipper effect at edges. With assumption that images have a slowly varying hue, the smooth hue transition (SHT) methods [1, 6, 20] interpolate the luminance (green) channel and chrominance (red and blue) channels differently. After recovering the green channel by bilinear interpolation, the red and blue channels are recovered by bi-linearly interpolating the red hue (the ratio of red to green) and blue hue (the ratio of blue to green). Although the SHT methods exploit the correlation between red, blue and green channels, they tend to cause large interpolation errors in the red and blue channels when green values abruptly change.

Since human visual systems are sensitive to the edge structures in an image, many adaptive demosaicking methods try to avoid interpolating across edges [2-3, 7, 11-12, 16, 18]. At each pixel the gradient is estimated, and the color interpolation is carried out directionally based on the

estimated gradient. Directional filtering is the most popular approach for color demosaicking that produces competitive results in the literature. The best known directional interpolation scheme is perhaps the second order Laplacian filter proposed by Hamilton and Adams [2-3, 11]. They used the second order gradients of blue and red channels as the correction terms to interpolate the green channel. The smaller of the two second order gradients in the horizontal and vertical directions is added to the average of the green samples along the chosen direction. Once the green samples are filled, the red and blue samples are interpolated similarly with the correction of the second order gradients of the green channel. Chang *et al.* [7] proposed a more complicated gradient-based demosaicking scheme. They computed a set of gradients in different directions in the 5×5 neighborhood centered at the pixel to be interpolated. A subset of these gradients is selected by adaptive threshold. At last the missing samples are estimated from the known samples located along the selected gradients. Recently, Ramanath and Snyder [18] proposed a bilateral filtering based scheme to denoise, sharpen and demosaick the image simultaneously. Alleysson *et al.* [4] wrote a color pixel as the sum of luminance and chrominance, and reconstructed the image by selecting the luminance and chrominance components in Fourier domain.

Another class of color demosaicking techniques is iterative schemes, which can also be combined with gradient-based methods. Kimmel developed a two-step iterative demosaicking process consisting of a reconstruction step and an enhancement step [13]. He calculated eight directional derivatives at each pixel based on its eight neighbors. Based on these edge indicators, the hue values are computed and the missing green, red and blue samples are then corrected iteratively by the ratio rule. Finally, an inverse color diffusion process is applied to the whole image for enhancement. Another iterative demosaicking scheme was proposed by Gunturk *et al.* [9]. Exploiting the fact that the three color channels of a natural image are highly correlated, Gunturk *et al.* reconstructed the color images by projecting the initial estimates onto so-called constraint sets. They first interpolated the image using Bilinear or other demosaicking methods, and then updated

the green channel by the high frequency information of red and blue channels. At last a wavelet-based iterative process was employed to update the high frequency details of the red and blue channels according to the green channel. Other demosaicking methods were also proposed, such as minimum mean square-error estimation [19], pattern matching [21], and median filtering [8].

In all color demosaicking techniques gradient analysis plays a central role in reconstructing sharp edges. However, the gradient estimate may not be robust when the input signal exceeds the Nyquist frequency. This is the main cause of color artifacts in demosaicked images. The challenge is to use statistically valid constraints to overcome the limit of Nyquist frequency. A common practice in color demosaicking is to exploit the correlation between the color channels. Since the three color channels of a natural image are highly correlated, the difference signal between the green channel and the red or blue channel constitutes a smooth (low-pass) process. Furthermore, we observe that this color difference signal is largely uncorrelated to the interpolation errors of gradient-guided color demosaicking methods, which are basically band-pass processes. These observations provide a rationale for estimating the color difference signals by linear minimum mean square-error estimation (LMMSE) method, which yields a good approximation to the optimal estimation in mean square-error sense. The LMMSE estimates are obtained in both horizontal and vertical directions, and then fused optimally to remove the demosaicking noise. Finally, the full-resolution three color channels are reconstructed from the LMMSE filtered difference signals. The experimental results show that the new color demosaicking technique significantly outperforms the state-of-the-art methods both in PSNR measure and visual perception.

This paper is structured as follows. In Section II we introduce the notions of primary difference signal (PDS) and the directional demosaicing noises. Section III presents the LMMSE technique of estimating primary difference signals in both horizontal and vertical directions. Section IV describes how these two directional estimates can be optimally fused into a more robust estimate. Then in Section V the chrominance channels are interpolated based on the estimated PDS and luminance

channel. Section VI gives the experimental results and Section VII concludes.

II. Primary Difference Signal and Directional Demosaicing Noise

Table 1. The correlation coefficients of all pairs of primary color channels. c_{rg} is the correlation coefficient of green and red channels; c_{bg} is the correlation coefficient of green and blue channels; and c_{rb} is the correlation coefficient of red and blue channels.

Images	1	2	3	4	5	6	7	8	9
c_{rg}	.9871	.9284	.9726	.9746	.9947	.9976	.9796	.9965	.9790
c_{bg}	.9878	.9891	.9803	.9713	.9985	.9928	.9980	.9821	.9569
c_{rb}	.9540	.9243	.9346	.9492	.9921	.9837	.9711	.9760	.9335
Images	10	11	12	13	14	15	16	17	18
c_{rg}	.9952	.9955	.9952	.9693	.9991	.9951	.9924	.9929	.9823
c_{bg}	.9910	.9892	.9967	.9942	.9921	.9854	.9940	.9965	.9823
c_{rb}	.9845	.9785	.9884	.9589	.9873	.9694	.9834	.9871	.9629

In order for a color demosaicking algorithm to recover high frequency features beyond the designed Nyquist frequency of the CFA, it has to rely on some additional statistical property or constraint(s) about the input color signals. A commonly exploited property is the correlation between the sampled primary color channels: red, green, and blue. In order to utilize this property in demosaicking, let us examine the relationships between the green and red channels, and between the green and blue channels. There are multiple reasons for why the green channel plays a key role in our estimation of missing color samples. First, the green channel has twice as many samples as the other two channels in the ubiquitous Bayer mosaic pattern, which is by far the prevailing CCD sensor design. Second, the sensitivity of the human visual system peaks at the green wavelength. Third, the green is closer to red and to blue than the difference between red and blue in wavelength. Table 1 lists the average correlation coefficients between all pairs of primary color channels measured over a set of 18 color test images shown in Fig.2. Clearly, the green-red and green-blue correlations are appreciably and consistently greater than the red-blue correlation.

Figure 2. Test images used in this paper.

(1)   (2)   (3)

(4)   (5)   (6)

(7)   (8)   (9)

(10)   (11)   (12)

(13)   (14)   (14)

(15)   (17)   (18)

In the color demosaicking literature, two assumptions were made on green-red and green-blue relations: equal ratio [1, 6, 13, 20] and equal difference [2-3, 7, 11]. The former assumption holds for mosaic CCD data prior to gamma correction, while the latter assumption is closer to the reality for gamma corrected mosaic CCD data. In this paper, we assume the difference images between the green and red channels, and between the green and blue channels to be low-pass signals, which are referred in the sequel as *primary difference signals* (PDS), and denoted by (referring to Fig. 1)

$$\Delta_{g,r}(n) = G_n - R_n; \qquad \Delta_{g,b}(n) = G_n - B_n \qquad (2\text{-}1)$$

where n is the position index of the pixels. The term is used because (2-1) represents two images whose pixel values are differences between corresponding green and red/blue samples.

For all reasons above, we demosaick the green channel first and then other two channels as many other researchers. Namely, we estimate the missing green samples under the assumption that $\Delta_{g,r}$ and $\Delta_{g,b}$ are smooth signals (some power spectrum density functions of $\Delta_{g,r}$ and $\Delta_{g,b}$ are plotted in Section III to support this assumption). The quality of final full color reconstruction largely hinges on the estimation accuracy of the missing green samples in the Bayer pattern, because the reconstructed green channel has an anchor affect on subsequent steps of demosaicing the red and blue channels as we will see in Section V. We estimate PDS $\Delta_{g,r}$ and $\Delta_{g,b}$ rather than individual color channels directly because random processes $\Delta_{g,r}$ and $\Delta_{g,b}$ have some statistical properties that can be exploited to aid demosaicking. In particular, we are interested in how the demosaicking noise relates to $\Delta_{g,r}$ and $\Delta_{g,b}$.

One of the well known and most effective color demosaicking filters is the second-order directional Laplacian filter of Adams and Hamilton [2-3, 11], which is also based on the assumption that $\Delta_{g,r}$ and $\Delta_{g,b}$ are constant in either horizontal or vertical direction. The key component of most existing adaptive demosaicing algorithms is the selection of the direction of color interpolation. In this paper, however, we make two separate estimates of a missing primary color sample in both

horizontal and vertical directions, and then optimally combine the two estimates (the topics of Sections III and IV).
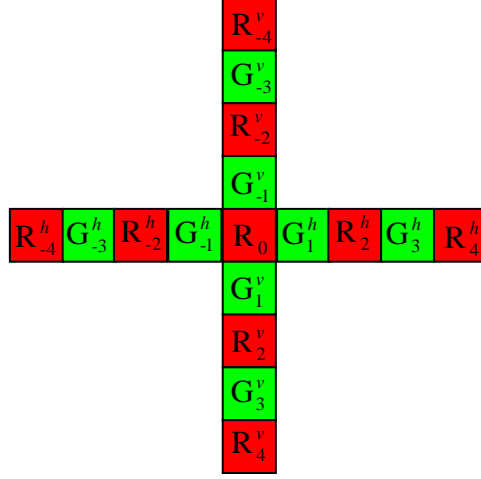

Figure 3. A row and a column of mosaic data that intersect at a red sampling position.

For concreteness and without loss of generality, we examine the configuration of the Bayer pattern as shown in Fig. 3: a column and a row of alternating green and red samples intersect at a red sampling position where the missing green value needs to be estimated. The results for the symmetric case of estimating the missing green values at the blue sampling positions of the Bayer pattern can be derived in the same way. We denote the red sample at the center of the window as R_0. Its interlaced red and green neighbors in horizontal direction are labeled as R_i^h, $i \in \{\cdots, -4, -2, 2, 4, \cdots\}$, and G_i^h, $i \in \{\cdots, -3, -1, 1, 3, \cdots\}$ respectively; similarly, the red and green neighbors of R_0 in vertical direction are R_j^v, $j \in \{\cdots, -4, -2, 2, 4 \cdots\}$, and G_j^v, $j \in \{\cdots, -3, -1, 1, 3, \cdots\}$ respectively. The sample R_0 at the intersection can be taken as R_0^h or R_0^v freely.

To get some coarse measurements of PDS $\Delta_{g,r}$ and $\Delta_{g,b}$, we first interpolate the missing green samples at red and blue pixels and then interpolate the missing red and blue samples at green samples. Any of the existed interpolation methods for color demosaicking [2-4, 6-9, 12-13, 16, 18] may be used. We adopt the second-order Laplacian interpolation filter for its easy implementation

and good performance. (But we stress that the following development is independent of the interpolation methods.) For any red original sample R_i^h or R_j^v, the corresponding missing green sample is interpolated as

$$\hat{G}_i^h = \frac{1}{2}\left(G_{i-1}^h + G_{i+1}^h\right) + \frac{1}{4}\left(2 \cdot R_i^h - R_{i-2}^h - R_{i+2}^h\right) \tag{2-2}$$

$$\hat{G}_j^v = \frac{1}{2}\left(G_{j-1}^v + G_{j+1}^v\right) + \frac{1}{4}\left(2 \cdot R_j^v - R_{j-2}^v - R_{j+2}^v\right) \tag{2-3}$$

Similarly, for any original green sample G_i^h or G_j^v, the corresponding missing red sample is interpolated as

$$\hat{R}_i^h = \frac{1}{2}\left(R_{i-1}^h + R_{i+1}^h\right) + \frac{1}{4}\left(2 \cdot G_i^h - G_{i-2}^h - G_{i+2}^h\right) \tag{2-4}$$

$$\hat{R}_j^v = \frac{1}{2}\left(R_{j-1}^v + R_{j+1}^v\right) + \frac{1}{4}\left(2 \cdot G_j^v - G_{j-2}^v - G_{j+2}^v\right) \tag{2-5}$$

Using the interpolated missing green and red values we obtain two estimates of the random process $\Delta_{g,r}$ in horizontal and vertical directions respectively:

$$\hat{\Delta}_{g,r}^h(i) = \begin{cases} \hat{G}_i^h - R_i^h, & G \text{ is interpolated} \\ G_i^h - \hat{R}_i^h, & R \text{ is interpolated} \end{cases} \text{ and } \hat{\Delta}_{g,r}^v(i) = \begin{cases} \hat{G}_i^v - R_i^v, & G \text{ is interpolated} \\ G_i^v - \hat{R}_i^v, & R \text{ is interpolated} \end{cases} \tag{2-6}$$

The estimation errors associated with $\hat{\Delta}_{g,r}^h$ and $\hat{\Delta}_{g,r}^v$ are

$$\begin{cases} \varepsilon_{g,r}^h = \Delta_{g,r} - \hat{\Delta}_{g,r}^h \\ \varepsilon_{g,r}^v = \Delta_{g,r} - \hat{\Delta}_{g,r}^v \end{cases} \tag{2-7}$$

We regard $\hat{\Delta}_{g,r}^h$ and $\hat{\Delta}_{g,r}^v$ to be two observations of $\Delta_{g,r}$, and accordingly $\varepsilon_{g,r}^h$ and $\varepsilon_{g,r}^v$ to be the corresponding *directional demosaicking noises*, and rewrite (2-7) as

$$\begin{cases} \hat{\Delta}_{g,r}^h = \Delta_{g,r} - \varepsilon_{g,r}^h \\ \hat{\Delta}_{g,r}^v = \Delta_{g,r} - \varepsilon_{g,r}^v \end{cases} \tag{2-8}$$

Now the task is to obtain an optimal estimate of $\Delta_{g,r}$ from the two observation sequences $\left\{\hat{\Delta}_{g,r}^h\right\}$

and $\left\{ \hat{\Delta}^{v}_{g,r} \right\}$, and then consequently derive the missing green values. The estimation algorithm will be developed in Section III.

To simplify the notations, we denote by x the true PDS signal $\Delta_{g,r}$, and by y the associated observation $\hat{\Delta}^{h}_{g,r}$ or $\hat{\Delta}^{v}_{g,r}$, and by υ the associated demosaicking noise $\varepsilon^{h}_{g,r}$ or $\varepsilon^{v}_{g,r}$, namely

$$y(n) = x(n) + \upsilon(n) \tag{2-9}$$

The optimal minimum mean square-error estimation (MMSE) of x is

$$\hat{x} = E[x/y] = \int x p(x/y)dx. \tag{2-10}$$

However, the MMSE estimation is very difficult, if possible at all, because $p(x/y)$ is seldom known in practice. Instead we use the linear minimum mean square-error estimation (LMMSE) technique to estimate x from y, which is a good approximation to MMSE but more amenable to efficient implementation. Particularly, if $x(n)$ and $\upsilon(n)$ are locally Gaussian processes (a reasonable assumption for many natural signals), then the spatially adaptive LMMSE developed in Section III will be equivalent to MMSE [14].

The LMMSE of x is computed as

$$\hat{x} = E[x] + \frac{Cov(x, y)}{Var(y)}(y - E[y]). \tag{2-11}$$

Empirically we found that the demosaicking noises $\varepsilon^{h}_{g,r}$ and $\varepsilon^{v}_{g,r}$ are zero-mean random process, and they are almost uncorrelated with $\Delta_{g,r}$. This can be seen in Table 2 that lists the correlation coefficient c_h between $\varepsilon^{h}_{g,r}$ and $\Delta_{g,r}$, and the correlation coefficient c_v between $\varepsilon^{v}_{g,r}$ and $\Delta_{g,r}$ for the test images in Fig. 2 (the mosaic data of them are simulated by subsampling with the CFA of the Bayer pattern), in which c_h and c_v are indeed very close to zero. Consequently, we can simplify (2-11) to

$$\hat{x} = \mu_x + \frac{\sigma_x^2}{(\sigma_x^2 + \sigma_\upsilon^2)}(y - \mu_x) \tag{2-12}$$

where $\mu_x = E[x]$, $\sigma_x^2 = Var(x)$, $\sigma_v^2 = Var(v)$.

Table 2. The lack of correlation between PDS $\Delta_{g,r}$ and the demosaicking noises $\varepsilon_{g,r}^h$ and $\varepsilon_{g,r}^v$. c_h is the correlation coefficient between $\Delta_{g,r}$ and $\varepsilon_{g,r}^h$ (in horizontal direction), and c_v is the correlation coefficient between $\Delta_{g,r}$ and $\varepsilon_{g,r}^v$ (in vertical direction).

Images	1	2	3	4	5	6	7	8	9
c_h	0.0271	0.0654	0.0502	0.0647	0.0517	0.0410	0.0364	0.0355	0.0562
c_v	0.0390	0.0305	0.0836	0.0648	0.0340	0.0200	0.0207	0.0176	0.0562
Images	10	11	12	13	14	15	16	17	18
c_h	0.0648	0.0298	0.0390	0.0422	0.0506	0.0274	0.0861	0.0855	0.0645
c_v	0.0173	0.0299	0.0412	0.0389	0.0531	0.0200	0.0716	0.0130	0.0512

Symmetrically, we can define the difference signal $\Delta_{g,b}$ between the green and blue channels, and its two estimates $\hat{\Delta}_{g,b}^h$ and $\hat{\Delta}_{g,b}^v$ in horizontal and vertical directions. The corresponding estimation errors $\varepsilon_{g,b}^h$ and $\varepsilon_{g,b}^v$ have the same properties as those of $\varepsilon_{g,r}^h$ and $\varepsilon_{g,r}^v$.

III. The Directional LMMSE of Primary Difference Signals

Having the knowledge of the statistical properties of the directional demosaicking noises $\varepsilon_{g,r}^h$ and $\varepsilon_{g,r}^v$, we now proceed to the LMMSE of PDS $\Delta_{g,r}$ by (2-12). To compute the LMMSE estimate $\hat{x}(n)$, we need to estimate the three parameters μ_x, σ_x and σ_v from observation data $y(n)$. And in order to make the estimate $\hat{x}(n)$ spatially adaptive, these parameters should be estimated locally in the neighborhood of $y(n)$.

We rely on the property that $x(n)$ is a low-pass process and $v(n)$ is a band-pass process to differentiate x from v in y. To verify this property let us examine the power spectrum density functions of $x(n)$ and $v(n)$. The power spectrum density function of a time series S is defined as the Fourier transform of the auto-correlation function of S:

$$f_p(\omega) = \frac{1}{2\pi} \sum_{k=-\infty}^{\infty} f_r(k) e^{-ik\omega} \tag{3-1}$$

where the sequence $f_r(k)$ is the auto-correlation function of S:

$$f_r(k) = E[S(n) \cdot S(n-k)] \qquad (3\text{-}2)$$

Since $f_r(k) = f_r(-k)$, (3-1) can be written as

$$f_p(\omega) = \frac{1}{2\pi}\left(f_r(0) + 2\sum_{k=1}^{\infty} f_r(k)\cos(k\omega) \right) \qquad (3\text{-}3)$$

The power spectrum density functions of x and υ are plotted in Fig. 4 and Fig. 5 for some typical natural images. In Fig. 4 the power spectrum of x for the first four images in Fig. 2 are plotted, and in Fig. 5 the corresponding power spectrum of υ are illustrated. Obviously, the power of x concentrates in low frequency band, whereas the power of υ spreads in relatively high frequency bands.
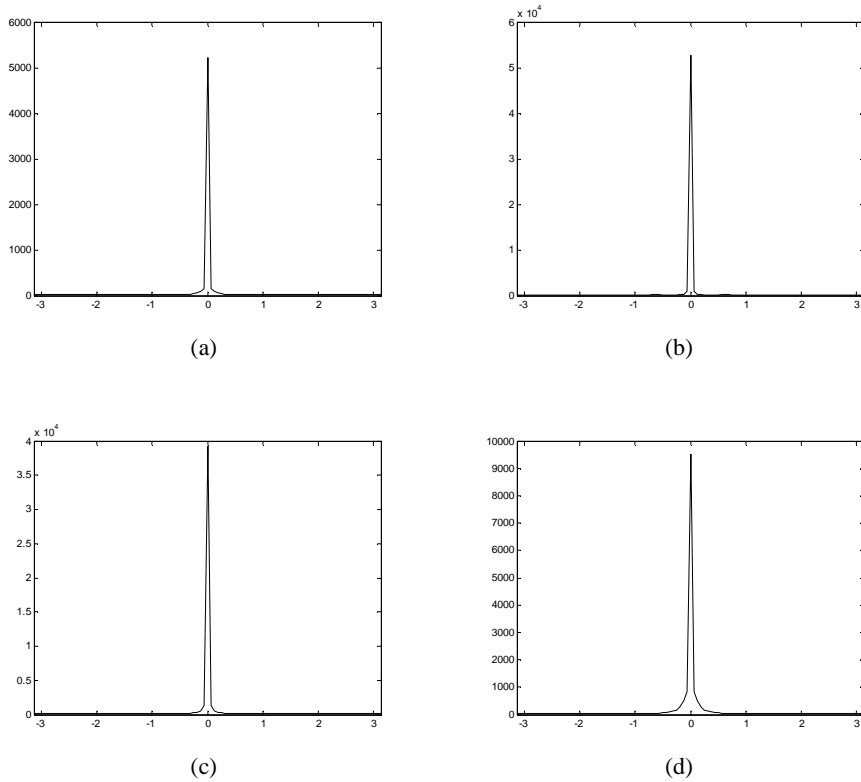

(a)

(b)

(c)

(d)

Figure 4. (a) ~ (d) are the power spectrum functions of the green-red difference signals in horizontal direction for the first four images in Fig. 2. The power spectrum functions in vertical direction are similar. It is clear that PDS is a low frequency dominated process.

(a-1)

(a-2)

(a-3)

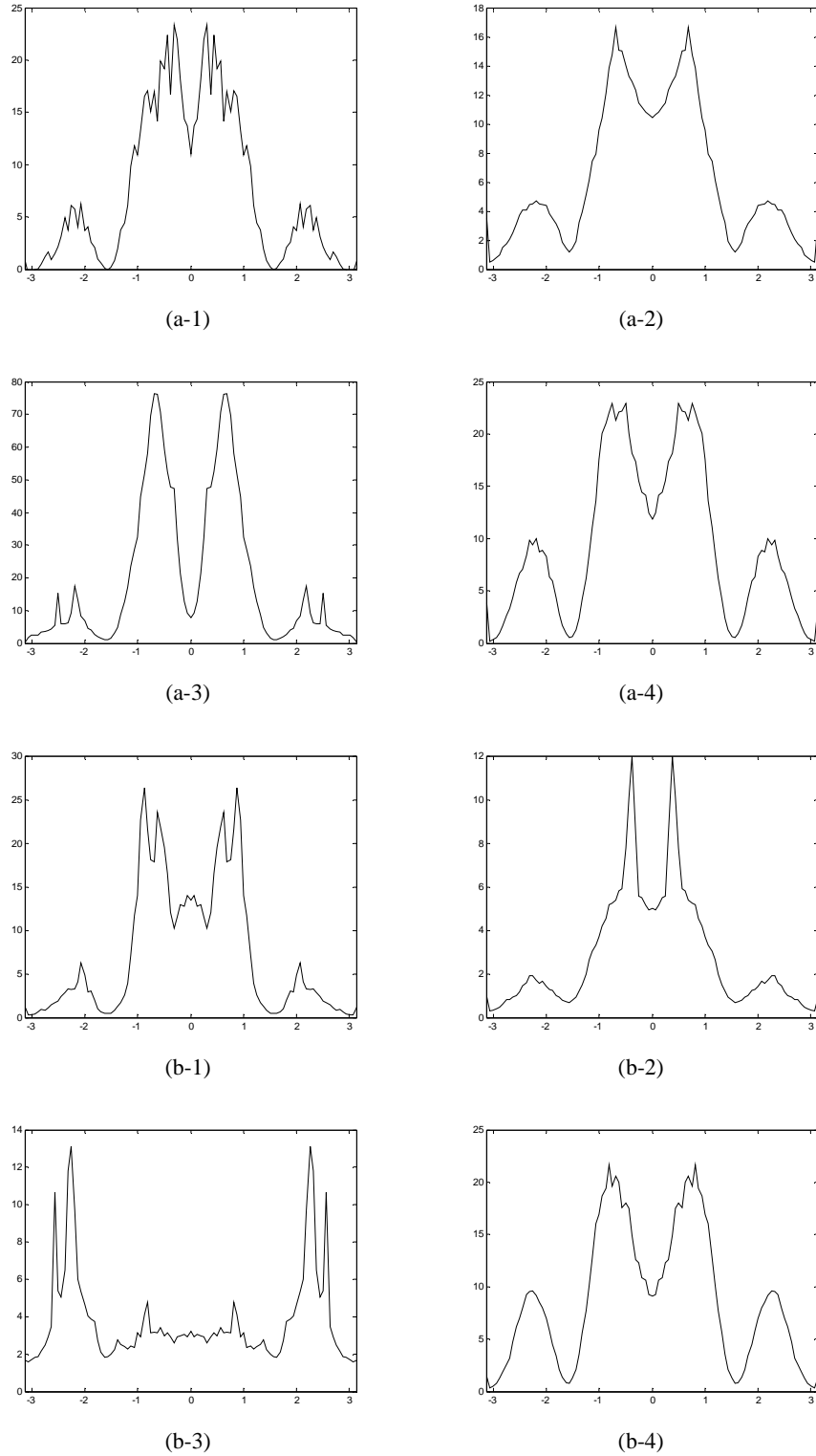(a-4)

(b-1)

(b-2)

(b-3)

(b-4)

Figure 5. (a-1) ~ (a-4) are the power spectrum functions of the estimation errors for the green-red PDS signal in horizontal direction for the first four images in Fig. 2; (b-1) ~ (b-4) are the power spectrum functions for the corresponding estimation errors in vertical direction. It can be seen that the estimation errors of PDS are band-pass processes.

Since x and υ have distinct power spectrum, passing y through a low-pass filter can remove the noises effectively. Denote by $\{h(k)\}$ the response sequence of a low-pass filter, we have

$$y_s(n) = (y * h)(n) = \sum_{k=-\infty}^{\infty} y(n-i) \cdot h(i) \qquad (3\text{-}4)$$

where "*" is the convolution operator. In this paper, we set $\{h(k)\}$ to be the Gaussian smooth filter, whose coefficients are

$$h(k) = \frac{1}{\sqrt{2\pi}\sigma} e^{-\frac{k^2}{2\sigma^2}} \qquad (3\text{-}5)$$

where parameter σ controls the shape of the filter response.

Assuming that the random process $x(n)$ is ergodic and stationary, its mean value $\mu_x(n)$ can be estimated by the neighboring data of $y(n)$. The low-pass filter output $y_s(n)$ is a weighted average of $y(n)$ and its neighbors, and it is much closer to $x(n)$ than $y(n)$. Denote by

$$Y_n^s = \left[y_s(n-L) \quad \cdots \quad y_s(n) \quad \cdots \quad y_s(n+L) \right] \qquad (3\text{-}6)$$

the $2L+1$ dimensional vector centered at $y_s(n)$, we estimate $\mu_x(n)$ as

$$\mu_x(n) = \frac{1}{2L+1} \sum_{k=1}^{2L+1} Y_n^s(k) \qquad (3\text{-}7)$$

and then we estimate $\sigma_x^2(n)$, the variance of $x(n)$, by

$$\sigma_x^2(n) = \frac{1}{2L+1} \sum_{k=1}^{2L+1} (Y_n^s(k) - \mu_x(n))^2 \qquad (3\text{-}8)$$

Denote by

$$Y_n = \left[y(n-L) \quad \cdots \quad y(n) \quad \cdots \quad y(n+L) \right] \qquad (3\text{-}9)$$

the $2L+1$ dimensional vector centered at $y(n)$. Since $y_s(n)$ is an approximation of $x(n)$ it follows that $y(n) - y_s(n)$ is an approximation of $\upsilon(n)$, thus we can estimate $\sigma_\upsilon^2(n)$, the variance of $\upsilon(n)$, by

$$\sigma_v^2(n) = \frac{1}{2L+1} \sum_{k=1}^{2L+1} (Y_n^s(k) - Y_n(k))^2 \tag{3-10}$$

For each sample $x(n)$ to be estimated, the corresponding parameters $\mu_x(n)$, $\sigma_x^2(n)$ and $\sigma_v^2(n)$ are computed and substituted into (2-12) to yield $\hat{x}(n)$, the nearly LMMSE estimate of $x(n)$. Let $\tilde{x}(n)$ be the estimation error of $x(n)$: $\tilde{x}(n) = x(n) - \hat{x}(n)$, the variance of $\tilde{x}(n)$ is

$$\sigma_{\tilde{x}}^2(n) = E[\tilde{x}^2(n)] = \sigma_x^2(n) - \frac{\sigma_x^2(n)}{(\sigma_x^2(n) + \sigma_v^2(n))} \tag{3-11}$$

IV. Optimal Fusion of the Directional LMMSE Estimates

Using the scheme developed in the previous section, two LMMSE estimates of a PDS signal $x(n)$ can be obtained, respectively in the horizontal and vertical directions, which are denoted by $\hat{x}_h(n)$ and $\hat{x}_v(n)$. Let $\tilde{x}_h(n)$ and $\tilde{x}_v(n)$ be the corresponding estimation errors, then

$$\begin{cases} \hat{x}_h(n) = x(n) - \tilde{x}_h(n) \\ \hat{x}_v(n) = x(n) - \tilde{x}_v(n) \end{cases} \tag{4-1}$$

The variances of estimation errors $\tilde{x}_h(n)$ and $\tilde{x}_v(n)$ are denoted by $\sigma_{\tilde{x}_h}^2(n)$ and $\sigma_{\tilde{x}_v}^2(n)$.

Either $\hat{x}_h(n)$ or $\hat{x}_v(n)$ exploits the correlation of $x(n)$ with its neighbors in a particular direction. A more accurate estimate of $x(n)$ can be obtained by fusing the two directional LMMSE estimates. We employ the weighted average strategy and let the fused estimate be

$$\hat{x}_w(n) = w_h(n) \cdot \hat{x}_h(n) + w_v(n) \cdot \hat{x}_v(n) \tag{4-2}$$

where $w_h(n) + w_v(n) = 1$. The weights $w_h(n)$ and $w_v(n)$ are determined to minimize the mean square-error of $\hat{x}_w(n)$:

$$\sigma_{\tilde{x}_w}^2(n) = E[\tilde{x}_w^2(n)] = E[(x(n) - \hat{x}_w(n))^2] \tag{4-3}$$

or

$$\sigma_{\tilde{x}_w}^2(n) = w_h^2(n) \cdot \sigma_{\tilde{x}_h}^2(n) + w_v^2(n) \cdot \sigma_{\tilde{x}_v}^2(n) + 2 \cdot w_h(n) \cdot w_v(n) \cdot E[\tilde{x}_h(n) \cdot \tilde{x}_v(n)] \tag{4-4}$$

Generally, the correlation between variables $\tilde{x}_h$ and $\tilde{x}_v$ is weak for a natural image, especially in the areas of edges and fine texture structures where the human visual system is sensitive to spatial resolution. In fact, if $\tilde{x}_h$ and $\tilde{x}_v$ are highly correlated, i.e., the two estimates $\hat{x}_h$ and $\hat{x}_v$ are close to each other, then $\hat{x}_w$ varies little in w_h and w_v anyways.

Assuming that $\tilde{x}_h$ and $\tilde{x}_v$ are approximately uncorrelated, the magnitude of the last term in the right side of (4-4) becomes negligible, or approximately

$$
\begin{aligned}
\sigma_{\tilde{x}_w}^2(n) &\approx w_h^2(n) \cdot \sigma_{\tilde{x}_h}^2(n) + w_v^2(n) \cdot \sigma_{\tilde{x}_v}^2(n) \\
&= w_h^2(n) \cdot (\sigma_{\tilde{x}_h}^2(n) + \sigma_{\tilde{x}_v}^2(n)) + \sigma_{\tilde{x}_v}^2(n) - 2 \cdot w_h(n) \cdot \sigma_{\tilde{x}_v}^2(n)
\end{aligned}
\tag{4-5}
$$

To minimize $\sigma_{\tilde{x}_w}^2(n)$, we let the partial differential of $\sigma_{\tilde{x}_w}^2(n)$ with respect to $w_h(n)$ be zero, namely

$$
\frac{\partial \sigma_{\tilde{x}_w}^2(n)}{\partial w_h(n)} = 2 \cdot w_h(n) \cdot (\sigma_{\tilde{x}_h}^2(n) + \sigma_{\tilde{x}_v}^2(n)) - 2 \cdot \sigma_{\tilde{x}_v}^2(n) = 0
\tag{4-6}
$$

Finally we have

$$
w_h(n) = \frac{\sigma_{\tilde{x}_v}^2(n)}{\sigma_{\tilde{x}_h}^2(n) + \sigma_{\tilde{x}_v}^2(n)}, \quad w_v(n) = \frac{\sigma_{\tilde{x}_h}^2(n)}{\sigma_{\tilde{x}_h}^2(n) + \sigma_{\tilde{x}_v}^2(n)}
\tag{4-7}
$$

Substituting (4-7) into (4-2) yields $\hat{x}_w(n)$, the optimally weighted estimate of $\hat{x}_h(n)$ and $\hat{x}_v(n)$. The MSE of the optimal estimate $\hat{x}_w(n)$ is

$$
\sigma_{\tilde{x}_w}^2(n) = \frac{\sigma_{\tilde{x}_h}^2(n)\sigma_{\tilde{x}_v}^2(n)}{\sigma_{\tilde{x}_h}^2(n) + \sigma_{\tilde{x}_v}^2(n)}
\tag{4-8}
$$

Obviously $\sigma_{\tilde{x}_w}^2(n)$ is less than either of $\sigma_{\tilde{x}_h}^2(n)$ and $\sigma_{\tilde{x}_v}^2(n)$.

Using the method described in Sections III and IV, we compute, for each red pixel position R_n and each blue pixel position B_n, the directional weighted estimates of the green-red PDS signal $\Delta_{g,r}(n)$ and the green-blue PDS signal $\Delta_{g,b}(n)$. Then we can recover the green channel of the Bayer CFA image by estimating the missing green samples as

$$\hat{G}_n = R_n + \Delta_{g,r}(n) \text{ or } \hat{G}_n = B_n + \Delta_{g,b}(n) \qquad (4\text{-}9)$$

Compared with the red and blue channels of a Bayer CFA image, the green channel preserves much more detail of the image and hence is more important for the human visual system. Furthermore, the interpolation quality of red and blue channels, which is the subject of the next section, also depends on the estimation accuracy of the green channel.

V. The Demosaicking of the Chrominance Channels

In the previous two sections we showed how to remove the demosaicking noise in the green channel by directional LMMSE filtering of PDS and optimal fusing of the resulting directional LMMSE estimates. Once the robust green estimates are obtained for all pixels, they can guide, in conjunction with the PDS estimates, the demosaicking of the red and blue channels. This is accomplished in the following two steps.

A. Interpolation of missing red (blue) samples at the blue (red) sample positions
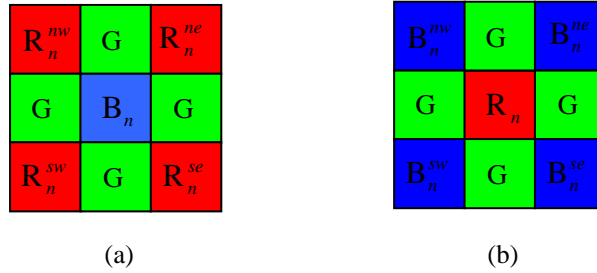

(a)   (b)

Figure 6. (a) A blue sample and its four nearest red neighbors. (b) A red sample and its four nearest blue neighbors.

We first interpolate the missing red sample at a blue pixel B_n. Referring to Fig. 6 (a), we denote by R_n^{nw}, R_n^{sw}, R_n^{ne} and R_n^{se} the four nearest red neighbors of the blue sample position B_n, where the superscripts are directional notations for northwestern, southwestern, northeastern and southeastern. Note that R_n^{nw}, R_n^{sw}, R_n^{ne}, R_n^{se} and B_n are all original samples in the Bayer pattern.

The estimated green samples at these positions are denoted by $\hat{G}_n$, $\hat{G}_n^{nw}$, $\hat{G}_n^{sw}$, $\hat{G}_n^{ne}$ and $\hat{G}_n^{se}$

respectively. The available four green-red difference values are represented as $\Delta_{n,gr}^{nw}$, $\Delta_{n,gr}^{sw}$, $\Delta_{n,gr}^{ne}$

and $\Delta_{n,gr}^{se}$. The estimate $\hat{R}_n$ of the missing red sample is to be computed.

We interpolate the green-red PDS signal at the blue sample position B_n as the average of the

four available green-red differences, namely

$$\Delta_{n,gr} = \frac{\Delta_{n,gr}^{nw} + \Delta_{n,gr}^{se} + \Delta_{n,gr}^{ne} + \Delta_{n,gr}^{sw}}{4} \tag{5-1}$$

Then the missing red sample is estimated as

$$\hat{R}_n = \hat{G}_n - \Delta_{n,gr} \tag{5-2}$$

Similarly, the missing blue samples at the red sample positions R_n (referring to Fig. 6 (b)) can

be interpolated. The four green-blue difference values in the northwestern, southwestern,

northeastern and southeastern of R_n are available, and they are averaged to interpolate the green-

blue PDS signal $\Delta_{n,gb}$ at position R_n. The missing blue sample is then estimated as

$\hat{B}_n = \hat{G}_n - \Delta_{n,gb}$.

B. Interpolation of missing red/blue samples at the green sample positions
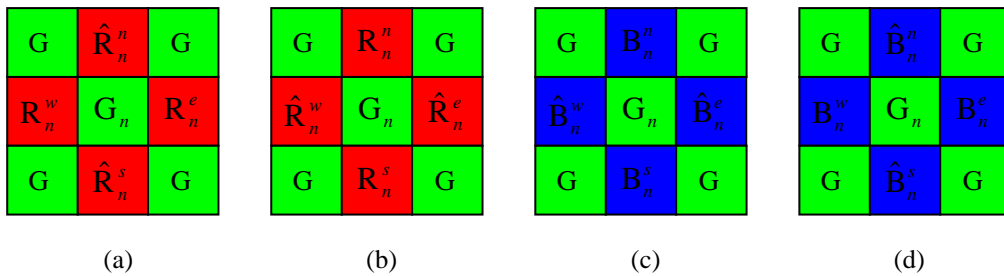

(a)　　　　　(b)　　　　　(c)　　　　　(d)

Figure 7. (a) ~ (b) A green sample and its two original and two estimated red neighbors. (c) ~ (d) A green sample and its two original and two estimated blue neighbors.

After the missing red/blue samples at the blue/red positions have been filled, we arrive at the

four cases depicted by Fig. 7. As before, the samples are estimated ones if marked by "^", and original ones otherwise. Due to the symmetry between red and blue samples in these four cases, we only need to discuss case (a). Given the green estimates $\hat{G}_n^n$, $\hat{G}_n^s$, $\hat{G}_n^e$ and $\hat{G}_n^w$ at the positions $\hat{R}_n^n$, $\hat{R}_n^s$, R_n^e, and R_n^w, we have the corresponding four green-red difference values, denoted by $\Delta_{n,gr}^n$, $\Delta_{n,gr}^s$, $\Delta_{n,gr}^e$ and $\Delta_{n,gr}^w$. As in the previous step, we compute the bilinear average of the green-red differences

$$\Delta_{n,gr} = \frac{\left(\Delta_{n,gr}^n + \Delta_{n,gr}^s + \Delta_{n,gr}^e + \Delta_{n,gr}^w\right)}{4} \qquad (5\text{-}3)$$

Then the missing red sample at green sample position G_n is estimated to be $\hat{R}_n = G_n - \Delta_{n,gr}$. Similarly, the missing blue sample at a green position G_n is estimated as $\hat{B}_n = G_n - \Delta_{n,gb}$.

By now we have filled in all the missing red/blue samples. The full color image is reconstructed. The presented demosaicking scheme first exploits the correlation between the green and red/blue channels to obtain good estimates of the missing green samples, and then estimates the missing red and blue samples by a simple and fast bilinear average operation on the green-red and green-blue PDS signals.

VI. Experimental Results

We implemented the proposed LMMSE color demosaicking algorithm, and tested it on a large number of natural color images. In this section we present our experimental results for the eighteen images of Fig. 2, and compare them with the methods of Hamilton *et al.* [2], Chang *et al.* [7] and Gunturk *et al.* [9], which are among the most popular schemes. The results reported in the recent paper of [9] were better than the previously published algorithms, especially for the red and blue channels. In the implementation of our scheme, the standard deviation of the Gaussian smooth filter, σ (referring to (3-5)), was set around 2, and the parameter L (referring to (3-6) and (3-9)) was set

to 4. In Table 3, the peak signal to noise ratios (PSNR) of the demosaicked images by the four methods are listed. The results of the method in [9] are duplicated from that paper. They were originally reported by mean square error (MSE) and we transformed them into PSNR by $\text{PSNR} = 10\log_{10}(255^2 / \text{MSE})$.

Table 3. The PSNR (dB) results of the proposed method and the other methods.

Images	1			2			3			4		
channels	R	G	B	R	G	B	R	G	B	R	G	B
Method in [2]	33.67	38.37	33.75	35.14	39.48	36.46	29.63	33.21	29.58	31.79	35.90	31.81
Method in [7]	30.06	38.57	30.24	36.33	40.70	37.96	29.16	34.42	29.17	32.44	35.53	32.45
Method in [9]	40.03	40.89	38.77	38.85	39.04	39.19	--	--	--	37.93	38.75	35.66
Proposed	41.17	42.91	39.31	37.75	43.30	41.07	34.17	39.58	33.95	37.98	40.99	36.69
Images	5			6			7			8		
channels	R	G	B	R	G	B	R	G	B	R	G	B
Method in [2]	37.50	41.53	37.11	35.86	39.67	35.91	30.90	34.70	30.99	27.71	30.68	27.43
Method in [7]	36.59	41.79	36.51	34.56	40.50	34.60	29.60	36.09	29.71	29.08	32.09	28.66
Method in [9]	42.63	42.89	39.82	42.14	43.30	40.91	37.65	39.59	37.47	34.45	36.35	33.22
Proposed	43.70	45.45	40.49	43.57	45.84	42.41	38.01	40.84	38.45	35.60	36.91	33.85
Images	9			10			11			12		
channels	R	G	B	R	G	B	R	G	B	R	G	B
Method in [2]	32.31	34.88	31.28	28.78	33.48	28.69	32.39	36.07	32.40	37.53	41.37	36.90
Method in [7]	33.59	35.93	32.37	25.98	33.97	25.80	31.44	37.09	31.58	37.63	41.80	37.25
Method in [9]	37.41	38.05	35.68	35.47	37.57	34.53	38.62	40.58	37.61	42.32	42.50	40.59
Proposed	38.15	39.01	35.82	35.34	39.02	35.30	40.20	42.42	38.70	43.26	45.13	40.64
Images	13			14			15			16		
channels	R	G	B	R	G	B	R	G	B	R	G	B
Method in [2]	33.44	37.17	33.76	36.32	39.77	35.45	32.94	36.38	32.65	34.52	37.87	34.02
Method in [7]	33.54	38.03	33.54	36.95	40.82	35.93	32.80	37.71	32.20	34.37	38.28	32.97
Method in [9]	39.00	40.46	38.61	41.18	39.60	38.47	39.06	40.16	37.60	36.85	38.89	36.59
Proposed	39.20	42.23	39.98	41.69	43.82	39.08	39.45	41.78	37.73	37.55	40.97	37.40
Images	17			18								
channels	R	G	B	R	G	B						
Method in [2]	38.00	42.35	37.98	38.18	42.18	38.10						
Method in [7]	37.16	42.74	37.37	38.72	42.08	38.75						
Method in [9]	42.83	43.13	41.77	42.53	42.51	39.96						
Proposed	42.30	46.43	42.79	41.86	45.34	40.98						

It can be seen from Table 3 that the estimates of the green channel are significantly improved by the proposed demosaicking algorithm. On average the improvement is 4.74dB, 4.04dB and 2.24dB higher than those of the other three algorithms respectively in PSNR. The new algorithm

also outperforms the other algorithms in red and blue channels as well. The margins of improvement in PSNR are 5.87dB and 6.23dB over the algorithm of [2] and the algorithm of [7] for the red channel, and respectively 5.06dB and 5.46dB for the blue channel. Compared with the algorithm of [9], the new algorithm achieves 0.46dB higher PSNR in the red channel and 0.84dB higher PSNR in the blue channel. One should keep in mind that the demosaicking results of [9] in the red and blue channels were obtained by costly eight iterations of wavelet-based filtering operations, while our results were obtained by simple bilinear interpolation of the primary difference signals. The computation and implementation complexities are considerably lower than [9].

In Fig. 8 ~ Fig. 13, some samples of the original and the demosaicked images by different methods ([2], [7] and the proposed) are shown for the purpose of subjective quality evaluation. For the visual results of [9] the reader can refer to the original paper. The proposed LMMSE-based demosaicking algorithm appears to produce visually more pleasant color images with color artifacts greatly suppressed.

VII. Conclusion

This paper presented a new color demosaicking technique of LMMSE directional filtering of the green-red and green-blue PDS signals. The missing green samples are estimated from the filtered PDS in both horizontal and vertical directions, and the two estimates are optimally fused. The resulting green channel is then used to guide the estimation of the missing red and blue samples. The experiments showed that the proposed color demosaicking algorithm significantly outperformed the current state of the art demosaicing methods both in PSNR measure and visual quality. Furthermore, the proposed algorithm is non-iterative, fast, and easy to implement.

References

[1] J. E. Adams, "Intersections between color plane interpolation and other image processing functions in electronic photography," *Proceedings of SPIE*, vol. 2416, pp. 144-151, 1995.

[2] J. E. Adams and J. F. Hamilton Jr., "Adaptive color plane interpolation in single color electronic camera," U. S. Patent, 5 506 619, 1996.

[3] J. E. Adams, "Design of practical color filter array interpolation algorithms for digital cameras," *Proceedings of SPIE*, vol. 3028, pp. 117-125, 1997.

[4] D. Alleysson, S. Süsstrunk and J. Hérault, "Color demosaicking by estimating luminance and opponent chromatic signals in the Fourier domain," *Proc. 10th Color Imaging Conference*, pp. 331-336, 2002.

[5] B. E. Bayer and Eastman Kodak Company, "Color Imaging Array," US patent 3 971 065, 1975.

[6] D. R. Cok and Eastman Kodak Company, "Signal Processing method and apparatus for producing interpolated chrominance values in a sampled color image signal," US patent 4 642 678, 1987.

[7] E. Chang, S. Cheung and D. Y. Pan, "Color filter array recovery using a threshold-based variable number of gradients," *Proceedings of SPIE*, vol. 3650, pp. 36-43, 1999.

[8] W. T. Freeman, "Method and apparatus for reconstructing missing color samples," U. S. Patents, 4 663 655.

[9] B. K. Gunturk, Y. Altunbasak and R. M. Mersereau, "Color plane interpolation using alternating projections," IEEE *Trans. Image Processing*, vol. 11, pp. 997-1013, 2002.

[10] H. S. Hou et al, "Cubic splines for image interpolation and digital filtering," *IEEE Trans. Acoustic, Speech and Signal Processing*, vol. ASSP-26, pp. 508-517, 1987.

[11] J. F. Hamilton Jr. and J. E. Adams, "Adaptive color plane interpolation in single sensor color electronic camera," U. S. Patent, 5 629 734, 1997.

[12] R. H. Hibbard, "Apparatus and method for adaptively interpolation a full color image utilizing luminance gradients," U. S. Patent 5 382 976, 1995.

[13] R. Kimmel, "Demosaicing: Image reconstruction from CCD samples," IEEE *Trans. Image Processing*, vol. 8, pp. 1221-1228, 1999.

[14] E. W. Karmen and J. K. Su, *Introduction to optimal estimation*, Springer-Verlag London Limited, 1999.

[15] P. Longère, Xuemei Zhang, P. B. Delahunt and Davaid H. Brainard, "Perceptual assessment of demosaicing algorithm performance," *Proc. of IEEE*, vol. 90, pp. 123-132, 2002.

[16] C. A. Laroche and M. A. Prescott, "Apparatus and method for adaptively interpolating a full color image utilizing chrominance gradients," U. S. Patent 5 373 322, 1994.

[17] William K. Pratt, *Digital Image Processing*, John Wiley & Sons, 2nd edition, April 1991.

[18] R. Ramanath and W. E. Snyder, "Adaptive demosaicking," *Journal of Electronic Imaging*, vol. 12, No. 4, pp. 633-642, 2003.

[19] H. J. Trussel and R. E. Hartwing, "Mathematics for demosaicking," IEEE *Trans. Image Processing*, vol. 11, pp. 485-492, 2002.

[20] J. A. Weldy, "Optimized design for a single-sensor color electronic camera system," *Proceedings of SPIE*, vol. 1071, pp. 300-307, 1988.

[21] X. Wu, W. K. Choi and Paul Bao, "Color restoration from digital camera data by pattern matching," *Proceedings of SPIE*, vol. 3018, pp. 12-17, 1997.
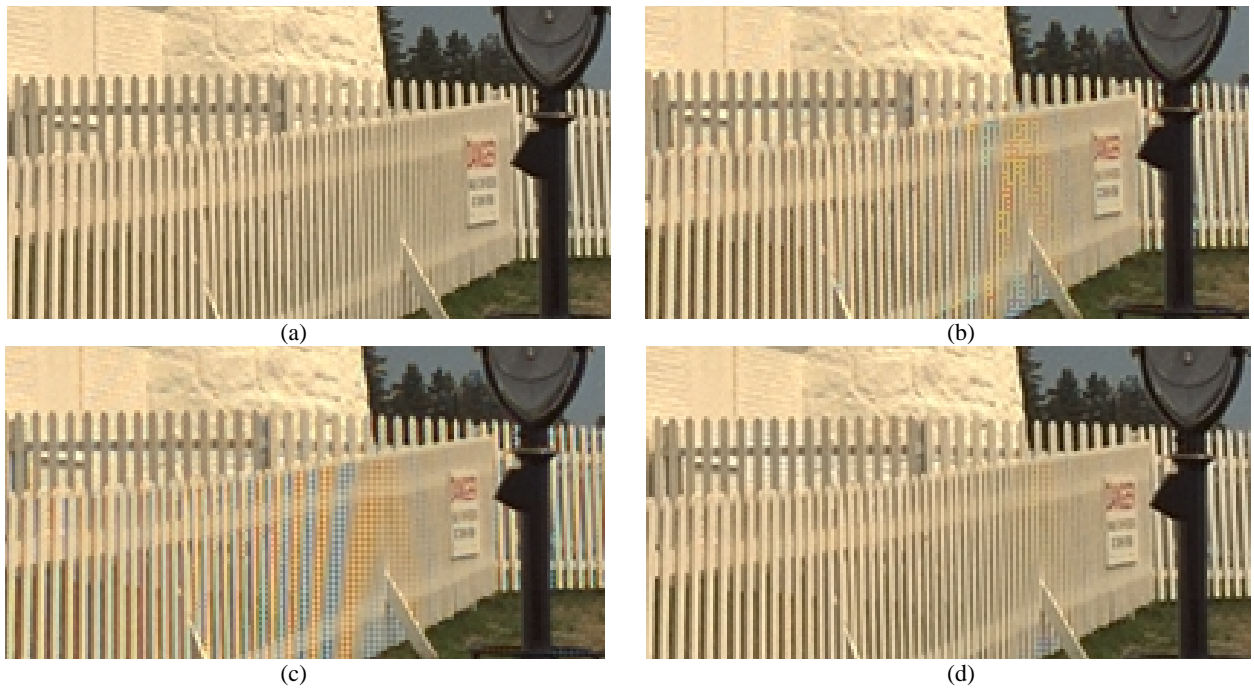
Figure 8. Demosaicked results of image 1 in Fig. 2: (a) Original; (b) Method in [2]; (c) Method in [7]; (d) The proposed method.
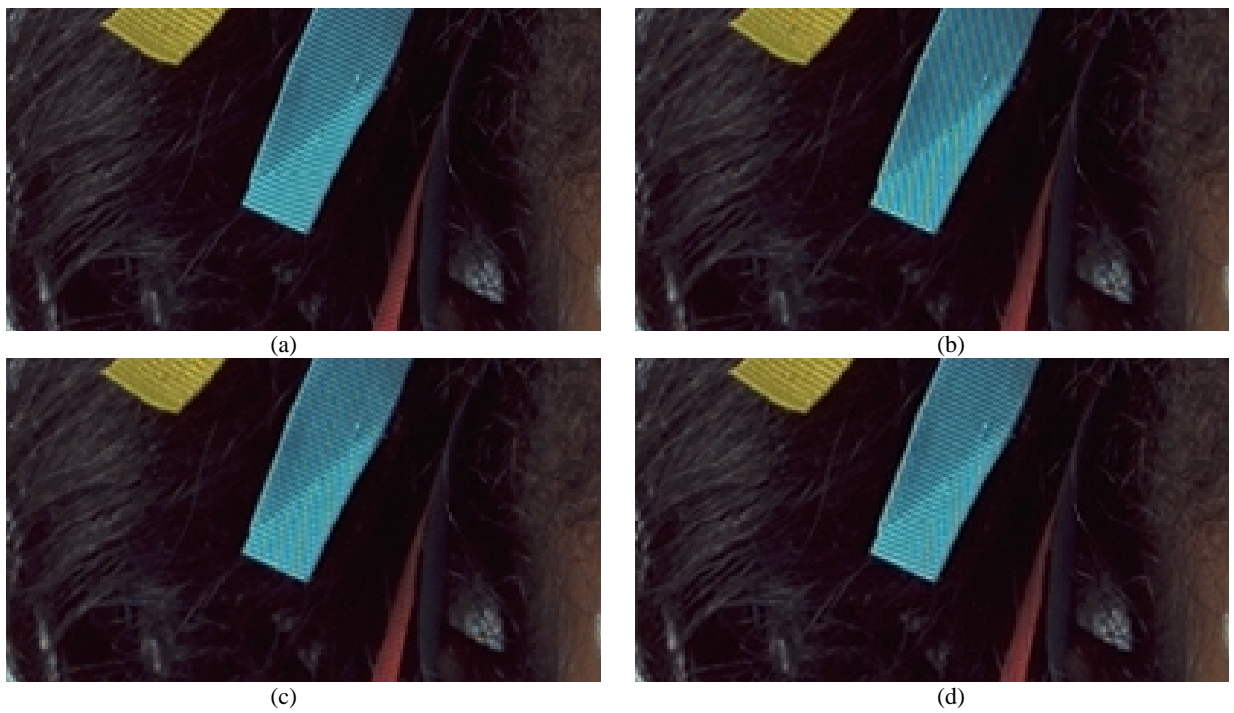

Figure 9. Demosaicked results of image 2 in Fig. 2: (a) Original; (b) Method in [2]; (c) Method in [7]; (d) The proposed method.
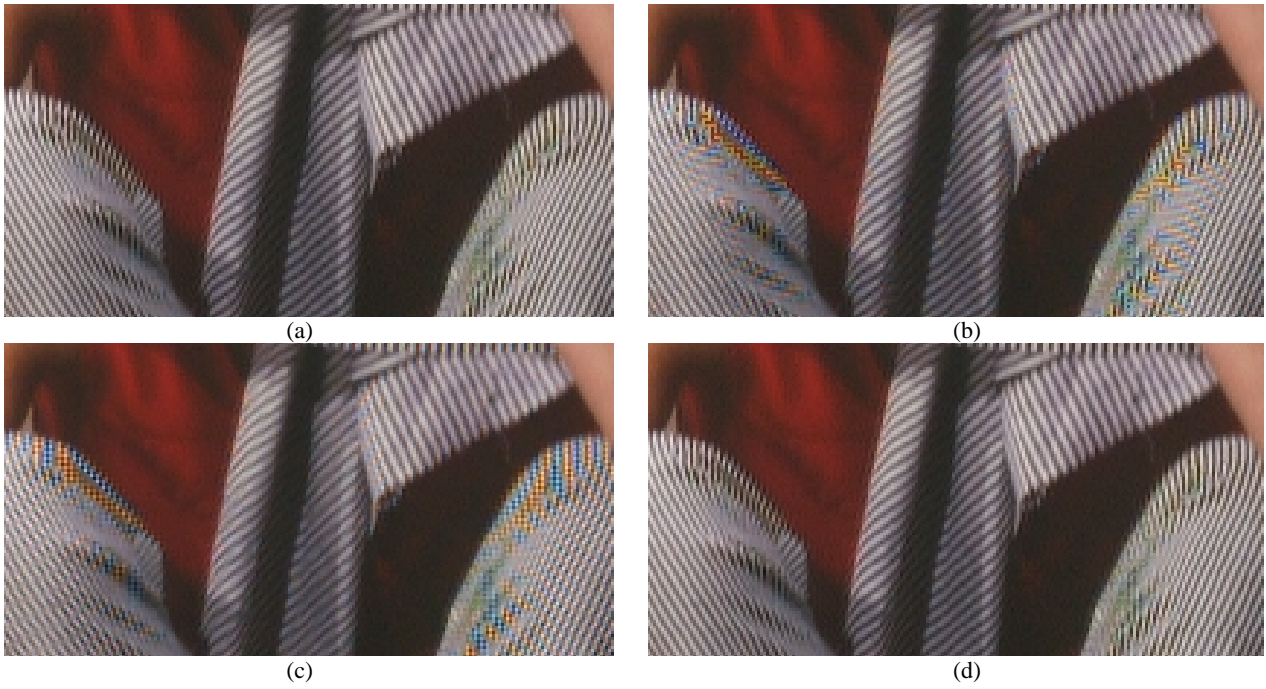
Figure 10. Demosaicked results of image 3 in Fig. 2: (a) Original; (b) Method in [2]; (c) Method in [7]; (d) The proposed method.
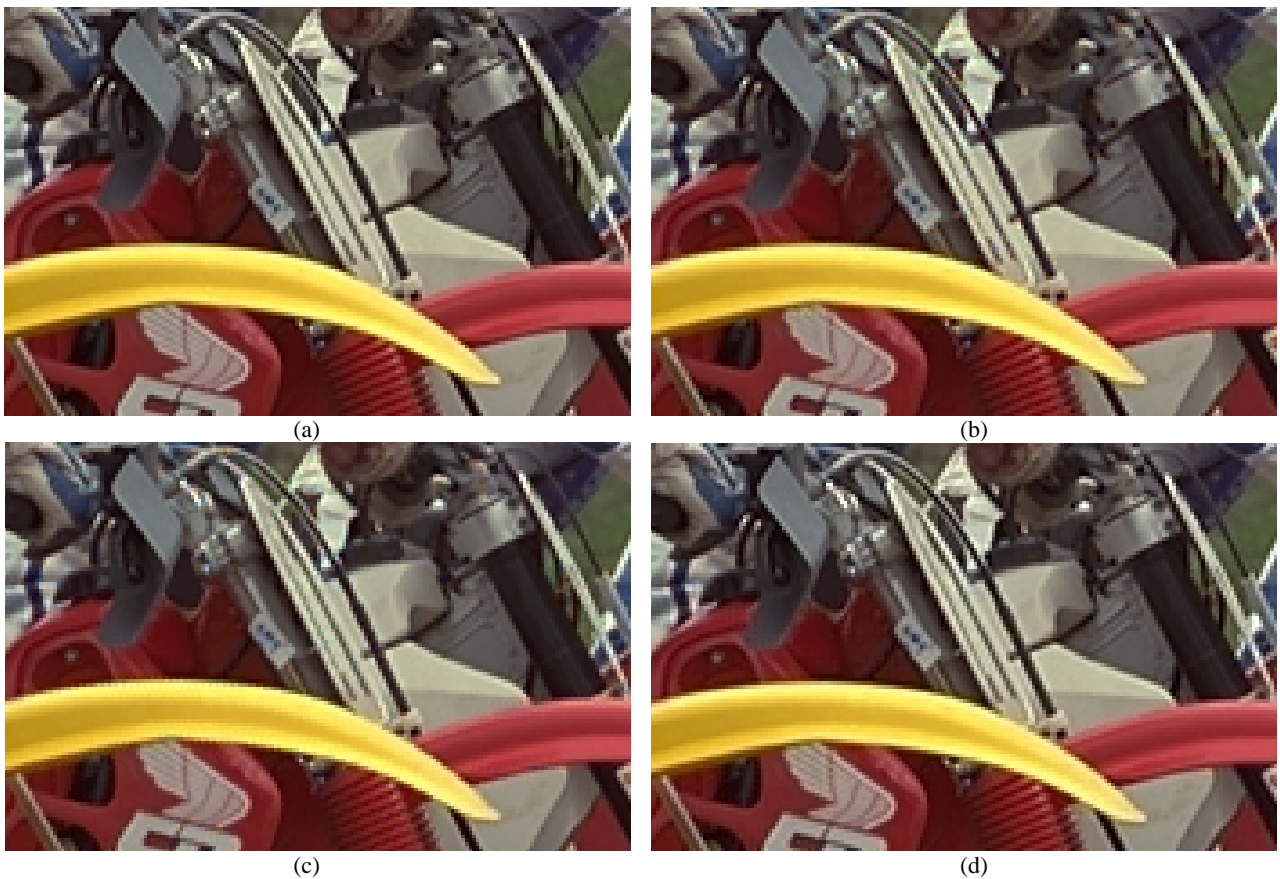

Figure 11. Demosaicked results of image 4 in Fig. 2: (a) Original; (b) Method in [2]; (c) Method in [7]; (d) The proposed method.
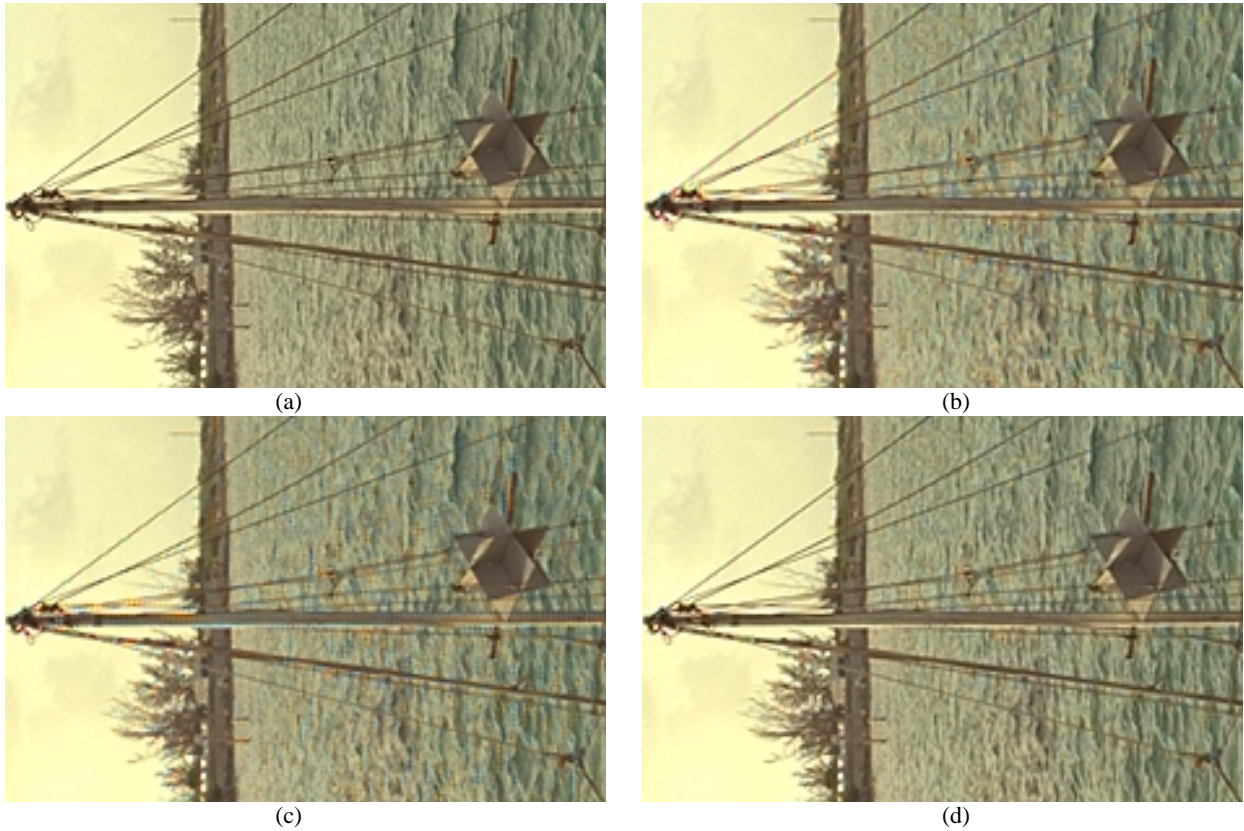
Figure 12. Demosaicked results of image 11 in Fig. 2: (a) Original; (b) Method in [2]; (c) Method in [7]; (d) The proposed method.

Figure 13. Demosaicked results of image 10 in Fig. 2: (a) Original; (b) Method in [2]; (c) Method in [7]; (d) The proposed method.